Hydroentangled Fabrics Manufactured from Photo-Irradiated Poly *para*-Phenylene Terephthalamide (PPTA) Fibres

TM Wright[d], CM Carr[a], C Grant[b], V Lilladhar[c] and SJ Russell[a]

[a] Nonwovens Research Group, School of Design, University of Leeds, UK

[b] Advanced Materials Engineering, School of Engineering, University of Bradford, UK

[c] Arvind-OG nonwovens, Ahmedabad, India

[d] Institut für Textilchemie und Textilphysik, Universität Innsbruck, Austria

Corresponding author

Tom Wright

Tel: +43 (0) 5572 28533

Email: Tom.Wright84@gmail.com (TM Wright)

Address: Höchsterstraße 73, 6850, Dornbirn, Austria

Abstract

Photo-irradiation of poly *para*-phenylene terephthalamide (PPTA) fibre is normally associated with deterioration of physical properties. Nonwoven fabrics produced from 100% photo-irradiated PPTA fibres might therefore be expected to yield fabrics with poorer mechanical properties compared to those produced from non-irradiated fibres. To test this hypothesis, the bursting strength of hydroentangled fabrics manufactured from photo-irradiated PPTA fibres was explored. Prior to fabric manufacture, virgin

PPTA staple fibres were photo-irradiated under controlled lighting conditions (xenon short arc lamp with a luminous flux of 13000 lm) for 0, 5, 10, 20, 40, 60 and 100 hr. The photo-irradiated fibres were then hydroentangled to produce nonwoven fabrics. Photo-irradiation exposure of PPTA fibre up to 30 $MJ.m^{-2}$ was not found to be detrimental to fabric bursting strength and at irradiation energies of 5-10 $MJ.m^{-2}$ a small, but statistically significant increase in fabric bursting strength was observed compared to fabrics manufactured from non-irradiated fibre. This may be linked to a change in the surface and skin properties of the PPTA photo-irradiated fibres identified by atomic force microscopy (AFM) following photo-irradiation.

Key words

Aramid, PPTA, Nonwoven, Photodegradation, AFM, Bursting strength testing.

1 Introduction

Poly *para*-phenylene terephthalamide (PPTA) fibres, known commercially as Kevlar (DuPont) and Twaron (Teijin) exhibit high tensile strengths (190 – 250 cN/tex[1]) and excellent chemical and thermal resistance[2]. This valuable combination of properties is due in part to the molecular structure in which the para position of the amide linkages allow for increased crystalline packing density. The meta position in aramid materials such as Nomex (DuPont) are associated with reduced crystalline packing, and lower tensile strength. PPTA fibres have a skin-core structure, wherein the core exhibits a more crystalline arrangement than the skin[3]. A radial order to the polymer units has also

been reported.[4,5] The highly crystalline core structure contributes to the high modulus of the material in fibre form, and the tensile strength and modulus are influenced by the relative proportion of the core and skin components. A thin skin section, making way for a thick core results in very high modulus but can be detrimental to fibre tensile strength as the large crystal units can also bring about inclusions of morphological defects such as cracks.[4]

Industrially, PPTA fibre is found in numerous applications including personal protection, composite reinforcement, ballistic and fire protection as well as the filtration of hot or volatile substances, amongst others. Given the valuable properties provided by the material, recycling of post-industrial PPTA waste is industrially attractive provided fibre properties do not substantially deteriorate compared to the virgin fibre. Fabrics containing recycled PPTA have been found to retain many useful properties, for example, Flambard et al.[6] reported fabrics containing recycled PPTA with excellent cut resistance. One industrially employed method of mechanically recycling PPTA is to retrieve manufacturing waste in the form of yarn or woven fabrics including weaver's waste and off-cuts from pattern cutting. Such wastes are cut in to dimensions suitable for mechanical processing and are then shredded (pulled) to produce staple fibre recyclate suitable to be used as a raw material for the manufacture of new products. This includes production of staple yarns in which recycled PPTA may be blended with virgin fibre prior to spinning and then the production of fabrics. PPTA fibre recyclate is also utilised as a feedstock for nonwoven fabric manufacture. The fibre recyclate is formed in to a web before being bonded to produce a stable fabric. Of the available

bonding methods, mechanical bonding by processes such as needling and hydroentangling, which rely upon fibre entanglement and friction to generate fabric strength, are particularly important because of the speed of production and the versatility of the processes.

One of the potential concerns in the use of PPTA fibre recyclate is the susceptibility of the material to photodegradation due to photo irradiation under to natural and artificial light in the UV and near UV part of the spectrum (300-450 nm).[7] Previous studies of PPTA photodegradation have mainly focused on ageing and exposing samples to artificial light exceeding 100 hr of accelerated degradation[8-10]. Deterioration in fibre mechanical properties occur as well as changes in chemical composition and structure leading to embrittlement, and surface artefacts. Li et al[11] studied the effects of shorter term UV irradiation of PPTA fibres and concluded that PPTA is highly sensitive to UV exposure even at low levels of irradiation. Changes were observed in the skin and surface morphology of PPTA fibres and an increase in surface wetting was also observed, which was attributed to greater surface roughness and the availability of oxygen-based functional groups on the fibre surfaces[11].

A potential advantage of post-industrial PPTA fibre waste utilised in the manufacture of nonwoven fabrics is that it is only likely to have received low levels of UV and light exposure compared to post consumer PPTA waste. However, the extent to which prior photo-irradiation of PPTA fibre influences final nonwoven fabric properties remains uncertain. Accordingly, in the present study, photo-irradiated and un-irradiated fibres were utilised as raw materials to manufacture nonwoven fabrics using an

industrially established mechanical bonding method known as hydroentangling. The purpose was to elucidate the effects of low levels of light exposure on final hydroentangled fabric bursting strength.

2 Methodology

2.1 Raw Materials and Web Manufacture

All experimental work was conducted using industrially available virgin PPTA staple fibre (Teijin Twaron 1078; 1.7 dtex; mean fibre length 58 mm; crimped) as the starting material. To ensure uniform photo-irradiation of the fibres prior to hydroentangling, virgin PPTA fibre was first formed in to carded batts and mechanically stabilised by pre-needling. Carded webs were prepared with a basis weight of 55 $g.m^{-2}$, the webs were prepared on a 0.5m wide Tatham worker-stripper nonwoven sample carding machine. Webs were parallel-laid using a 0.5 m wide lapper, to produce batts with an area of roughly 0.25 m^2. This relatively lightweight batt was formed to ensure uniform photo-irradiation during the subsequent aging procedure. To facilitate ease of handling, the batts were lightly pre-needled using a needle penetration depth of 12 mm and a very low punch density of 5.4 $punches.cm^{-2}$ using regular three-barbed needles (Specification: 15-18–42; Foster needle, USA). This loosely bonded fibrous assembly is referred to as a lightly pre-needled fabric.

2.2 Photo-Irradiation Procedure

Samples of the PPTA pre-needled fabric were then irradiated for different time periods of 0, 5, 10, 20, 40, 60 and 100 hr using a XBO 450 w/4 xenon short arc lamp with a luminous flux of 13000 lm. The configuration of the irradiation chamber allowed for an incident energy of 210 $W.m^{-2}$, roughly equivalent to a medium to high level of irradiation incident on the earth provided by the sun (the world meteorological organisation defines time of "sunshine" as the time that the surface receives at least 120 $W.m^{-2}$)[12]. The XBO lamp spectrum is given in Figure 1, this spectrum was used as it is a close approximation of a D65 daylight spectra. The irradiation energy levels ($MJ.m^{-2}$) were determined ($0 - 76\ MJ.m^{-2}$) based upon the sample dimensions, geometric position from the light source and the emitted energy. A non-irradiated PPTA pre-needled fabric was retained as a control sample and all samples were stored in black bags in a dark storage area prior to hydroentangling to minimise any extra environmental irradiation.

The irradiation energy (MJ) received by the PPTA was calculated by first calculating the light energy incident on the material in Lumens (lm), i.e. candela steradians (cd x Sr), which are given by the manufacturer and physical dimensions of the experiment for candela and steradians respectively. Lux was then calculated using Equation 1.

$$Lux = \frac{lm}{a} \qquad \text{Equation 1}$$

Where, lm is lumen and *a* is the area, this value is then converted to Watts.m^{-2} using the conversion factor of 0.00146 and finally multiplied by the exposure time to give the total energy in J.m^{-2}.

2.3 Bonding of Fibre Web Samples by Hydroentangling

The photo-irradiated PPTA pre-needled fabrics were hydroentangled using a 0.5 m wide pilot-line (STL Hydrolace) using the operating conditions in Table 1. Hydroentangling subjects the fibres in the web to kinetic energy delivered by an array of columnar, high-velocity water jets issuing from a row of small diameter, cone-capillary shaped nozzles.

Each web sample was hydroentangled sequentially on the face and back to promote uniform fibre entanglement throughout the structure. The fabrics were then dried for 5 minutes in a through-air oven at a temperature of 100°C.

2.4 Single fibre tensile testing

Single PPTA staple fibres were photo-irradiated up to a total irradiation energy of 9.3 MJ.m^{-2} with an irradiation power of 107.6 W.m^{-2} using an XBO 450 w/4 xenon short arc lamp operating with a luminous flux of 13000 lm. The fibres were mounted on small 20 mm x 20 mm square cardboard frames and glued at either end to hold them in place. The frames were then placed on a large plastic holder before being irradiated by the Xenon arc lamp irradiation box for time periods of t= 0, 4, 8, 16 and 24 hr equating to 0, 1.55, 3.1, 6.2 and 9.3 MJ.m^{-2} irradiation energy. Short exposure times were selected to gain a better understanding of any progressive change in fibre mechanical properties that might influence the way in which PPTA fibres respond during hydroentangling.

Tensile testing was based on BS EN ISO 13895:2003 using an Instron 1026 with a crosshead speed of 50 mm.min^{-1} and a gauge length of 20 mm. The specimens, retained in cardboard windows were mounted in the pneumatic jaws of the Instron. Once in position, the vertical sides of the windows were cut and the test was started. Twenty specimens for each sample were tested.

2.5 Atomic force microscopy (AFM)

All AFM experiments were carried out using an Asylum Research MFP-3D (Santa Barbara, CA) using AC160TS Olympus silicon cantilever probes with a tip radius (R_{tip}) of 25nm and a half cone angle of θ=36°, which were independently verified by scanning a standard calibration grid. The spring constant of the cantilever was calculated using the thermal method [13] via the in-built software. The inverse optical laser sensitivity (InvOLS) of the photodiode was calibrated by calculating the slope of tip deflection against the piezo Z-sensor displacement, by pressing against a hard silica surface over the experimental range of temperatures.

Fibres were attached to a standard microscope slide using silver conductive paint that allowed the fibre to be fixed, without damaging the surface (Figure 2). AFM images were captured using intermittent contact mode.

Force nanoindentations (n=100) were performed on the control and a photo-irradiated sample (9.3 MJ.m^{-2} irradiated single fibre). Maximum force was 3 µN at 2 µm.s^{-1}. Force-indentation plots were modelled using the linear elastic Hertzian theory for spherical contact (Equation 2).

$$F = \frac{4}{3}\frac{E}{1-\upsilon^2}h^{3/2}\sqrt{R}$$ Equation 2

Where *F* is the applied load, *h* is indentation depth, *E* is reduced modulus, υ is Poisson's ratio (assumed to be 0.5) and *R* is the effective radius between a round AFM tip (R_{tip}=25nm) and round fibril ($1/R = 1/R_{tip}+1/R_{fibril}$). Following nanoindentation, the surfaces were re-scanned to ensure that no plastic deformation had occurred.

As the AFM probe can be quantified in terms of its radii, AFM can be used as a nano-indenter with appropriate calibration of the cantilever spring constant. This set-up has been commonly used to calculate the elastic moduli of polyethylene terephthalate (PET) films[19], collagen fibrils [20]and agar gels[21]. Accurate modulus values using AFM nanoindentation techniques were found when indenting a reference elastomer surface with known mechanical properties[22].

2.6 Scanning Electron Microscopy (SEM) and kink-band quantification

Fabric samples photo-aged for 5, 10, 15 and 20 hr at 210 $W.m^{-2}$ equivalent to 3.79, 7.59, 11.38, 15.18 $MJ.m^{-2}$ irradiation energies together with the control sample were imaged. The samples were mounted onto aluminium stubs and sputter coated with gold, the micrographs were taken using a Carl Zeiss EVO® MA 15 Scanning Electron Microscope. Five images per sample were taken at 500X using a working distance range of 8-13mm. The images were taken at random locations in the specimens. The micrographs were then analysed using image analysis (Image ProPlus 6.2.1). The fibre length was

measured and the number of kink-bands were counted and reported via a kink-band index (K) defined in Equation 3.

$$K = \frac{Total\ number\ of\ kink\ bands}{Total\ length\ of fibre\ analysed} \qquad \text{Equation 3}$$

2.7 Determination of Fabric Bursting Strength

Tensile testing is commonly used to characterise fabric strength, but in the nonwoven fabrics studied in this work, uniaxial loading produced jaw breaks and excessive necking of specimens during testing resulting in unreliable data. Consequently, bursting strength was measured, in which multi-axial loading of the test specimen is employed. This method is recommended for the measurement of deformable materials such as nonwovens and reflects the mode of loading in many practical end uses. The ball burst method involves forcing a spherical metal former through a clamped specimen of the fabric (BS EN ISO 9073-5:2008). To avoid bridging of longer fibres in the fabric, the clamp diameter utilised in the bursting test was increased from 38.1 mm to 66.8 mm. To account for any small variations in web weight the bursting strength data was normalised by test area mass so that specific bursting strength[14] index could be reported.

3 Results and Discussion

3.1 Single fibre tensile properties

Despite the relatively short irradiation exposure times, Figure 3 indicates that the stress at break of single fibres decreased linearly with irradiation, which is in agreement with other studies.[9] This is likely to be a result of chain scission, end group formation and oxidation and further irradiation would be expected to result in a levelling of the tensile strength, possibly as a result of a saturation effect of the degradation products.[8,15]

Andrews and Young [16,17]reported that the initial rate of decrease in tensile strength, from the first data point to the second, can be greater than the rate of decrease for the remaining data points, which is also evident in the work by Li et al[11]. Such a trend cannot be confidently identified in Figure 3 despite the apparent large difference between the first and second data points between of 0 and 2 $MJ.m^{-2}$ (in comparison to the rest of the trend), although this may be worthy of further study.

Stress strain curves were obtained for all samples, and the average data is shown in Figure 4. No significant difference in modulus was observed, the mean values and standard deviations of the samples can be seen in Table 2. Although there was no significant change in elastic modulus as a result of increasing the irradiation ($P>0.05$), the reduction in tensile strength and elongation at break as a result of an irradiation energy of 9.3MJ was significant ($P<0.05$)

The absence of a significant difference in elastic modulus may be a consequence of the degradation being mainly confined to the skin of the fibre rather than the core,

which if affected would be expected to result in larger changes in fibre tensile properties.

3.2 Atomic Force Microscopy

Atomic force microscopy (AFM) allows nanoscale characterisation of polymer surfaces and under special conditions molecular resolution is possible[18]. Figure 5 shows AFM images of the two PPTA fibre surfaces prior to nanoindentation. Compared to the unaged samples, the aged surfaces were rougher more and developed prominent surface features.

Following the AFM testing, the reduced elastic modulus (Er) of the non-irradiated PPTA fibre surface was found to be 8.39 ± 1.09 GPa whereas the irradiated fibre had a modulus of 4.15 ± 0.48 GPa (mean ± standard deviation). Figure 6 shows the distinctly different distributions of the modulus results (n=100 indentations per fibre) for the non-irradiated and irradiated fibres.

This decrease in modulus is in keeping with findings by other researchers.[9,15,23,24] However, the present study has established that at low levels of irradiation, although a decrease in modulus is notable at the surface, the corresponding change in bulk modulus properties is relatively small as evident from the tensile stress – strain data. This further suggests that the short irradiation time mainly affected the skin component of the fibre in these experiments. Nevertheless, it is evident from this and previous studies, that irradiation negatively affects fibre mechanical properties and it would be

reasonable to expect this to translate in to nonwoven fabrics exhibiting inferior mechanical properties, compared to those composed of virgin fibres.

3.3 Scanning Electron Microscopy (SEM) and kink-band quantification

The degree of kink banding observed in the final hydroentangled fabrics increased with the level of irradiation of the PPTA fibres (Figure 7). In addition to kinkbands, SEM micrographs (Figure 8, Figure 9 and Figure 10) of the irradiated samples revealed increased surface roughness, which is consistent with the findings of Li et al.[11] Embrittlement and discoloration as a consequence of photodegradation was also reported by Carlsson *et al*.[8] An increase in kink banding as a result of increased embrittlement can give rise to ridging and thus surface roughening. Xing *et al.*[25] also noted brittle cracking of the surface structure suggesting an apparent increase in surface roughness as evidenced by Scanning Electron Microscopy (SEM) observations.

3.4 Fabric Bursting Strength

Because of the very different way in which hydroentangled fabrics are formed compared to woven and knitted textile fabrics it is instructive to understand how changes in PPTA fibre mechanical properties and surface roughness influence subsequent fabric bursting strength. Figure 11 shows the bursting strength of hydroentangled fabrics produced from irradiated PPTA fibres.

Interestingly, there was no reduction in fabric bursting strength following initial exposure of PPTA fibres to low irradiation energy levels of <20 $MJ.m^{-2}$ prior to bonding by hydroentangling. Surprisingly, a small but significant ($P<0.05$) increase in bursting

strength was initially observed, Figure 11. Subsequently, as the irradiation energy increased beyond 30 $MJ.m^{-2}$ up to about 76 MJ/m^2 a consistent reduction in fabric bursting strength occurred, which is consistent with what was originally anticipated based on existing scientific evidence regarding the influence of photo-irradiation on PPTA mechanical properties.[9,15,24]

Hydroentangling involves displacement and fibre entwinement to produce mechanical entanglements that increase frictional resistance and therefore the strength of the fabric. Ideally, this requires fibres to be flexible such that they can bend around relatively small radii and resist slippage following entanglement. Accordingly, it is conceivable that any reduction in fibre modulus, particularly wet modulus could assist fibre entanglement during hydroentangling increasing fabric strength. However, while a reduction in the modulus of PPTA fibre at the surface was detected by AFM, the elastic modulus determined by single fibre tensile testing (

Table **2**) indicated no significant change as a result of irradiation. The softening of fibre surfaces detected by AFM as a result of irradiation could potentially lead to a greater contact area between intersecting fibres as a result of deformation, increasing frictional resistance as fibres are forced in to closer proximity during hydroentangling. Additionally, the increased surface roughness in the irradiated PPTA fibres observed in Section 2.10 and the improved wettability noted by Li et al.[11] could also potentially modify fibre surface friction and therefore the strength of resulting fabrics. Such increases in surface roughness of PPTA fibre as a result of photodegradation have also been reported by both Carlsson *et al*.[8] and Xing *et al.*[25] who noted brittle cracking of the

surface structure suggesting an apparent increase in surface roughness as evidenced by Scanning Electron Microscopy (SEM) observations.

4 Conclusions

The tensile strength of virgin PPTA fibres reduced when subjected to irradiation at 210 $w.m^{-2}$ for up to 10 hr, equivalent to 7.6 $MJ.m^{-2}$. However, the burst strength of mechanically bonded hydroentangled fabric produced from lightly irradiated PPTA fibres was not negatively affected until irradiation energies exceeded 30 $MJ.m^{-2}$. At very low irradiation energies of 5-10 $MJ.m^{-2}$ a small increase in the burst strength of fabrics was observed compared to the non-irradiated control sample. This could not be explained in terms of reduced tensile modulus in the irradiated PPTA fibres, but may be linked to modifications of the surface and skin properties of the PPTA photo-irradiated fibres, such as a lower surface modulus and increased roughness, as detected by AFM and SEM respectively. These findings underline the potential for post-industrial PPTA recyclates to be utilised as raw materials in demanding nonwoven product applications provided UV-exposure is controlled before manufacture.

5 Acknowledgements

The authors wish to thank Aptec Textiles, UK for providing raw materials. The financial support of the Clothworkers' Foundation is gratefully acknowledged.

6 References

1 Teijin. *Twaron for heat and cut protection*, <http://www.teijinaramid.com/eCache/INT/24/140.pdf> (2011).

2 Yang, H. H. *Kevlar aramid fiber*. (Wiley, 1993).

3 Morgan, R. J., Pruneda, C. O. & Steele, W. J. The relationship between the physical structure and the microscopic deformation and failure processes of poly(p-phenylene terephthalamide) fibers. *Journal of Polymer Science: Polymer Physics Edition* **21** (1985).

4 Dobb, M. G. & Robson, R. M. Structural characteristics of aramid fibre variants. *Journal of Materials Science* **25**, 459-464 (1990).

5 Singletary, J., Davis, H. & Song, Y. The transverse compression of PPTA fibers. *Journal of Materials Science* **35**, 583-592 (2000).

6 Flambard. X, Ferreira. M, Vermeulen. B & S, B. Mechanical and Thermal Behaviors of First Choice, Second Choice and Recycled P-Aramid Fibers. *Journal of Textile and Apparel, Technology and Management* **3** (2003).

7 DuPont. *Technical Guide: Kevlar Aramid Fiber*.

8 Carlson, D. J., Gan, L. H. & Wiles, D. M. Photodegradation of Aramids. II. Irradiation in Air. *Journal of Polymer Science* **16**, 2365-2376 (1978).

9 Zhang, H. *et al.* Effects of solar UV irradiation on the tensile properties and structure of PPTA fiber. *Polymer Degradation and Stability* **91**, 2761-2767 (2006).

10 Brown. J.R, Browne. N.M, Burchill. P.J & G.T, E. Photochemical Ageing of Kevlar 49. *Textile Research Journal* **53**, 214 - 219 (1983).

11 Li, S., Gu, A., Xue, J., Liang, G. & Yuan, L. The influence of the short-term ultraviolet radiation on the structure and properties of poly (< i> p</i>-phenylene terephthalaramide) fibers. *Applied Surface Science* **265**, 519-526 (2013).

12 Organization, W. M. Measurement of meteorological variables: Measurement of sunshine duration. *Chapter 8* (2008).

13 Hutter, J. L. & Bechhoefer, J. Calibration of Atomic-Force Microscope Tips. *Review of Scientific Instruments* **64**, 1868-1873 (1993).

14 Jang, J. & Ryu, S. K. Physical property and electrical conductivity of electroless Ag-plated carbon fiber-reinforced paper. *Journal of Materials processing Technology* **180**, 66-73 (2006).

15 Brown, J. R., Browne, N. M., Burchill, P. J. & Egglestone, G. T. Photochemical Ageing of Kevlar 49. *Textile Research Journal* **53**, 214 - 219 (1983).

16 Andrews, M. C. & Young, R. J. Fragmentation of aramid fibres in single-fibre model composites. *Journal of Materials Science* **30**, 5607-5616, doi:10.1007/BF00356693 (1995).

17 Lin, L., Shen, Y. & Zhang, Q. Analysis of environmental impact on mechanical properties of aramid filaments. *Journal of Industrial Textiles* **42**, 489-500, doi:10.1177/1528083712446383 (2013).

18 Gross, L., Mohn, F., Moll, N., Liljeroth, P. & Meyer, G. The Chemical Structure of a Molecule Resolved by Atomic Force Microscopy. *Science* **325**, 1110-1114, doi:10.1126/science.1176210 (2009).

19 Grant, C. A., Alfouzan, A., Gough, T., Twigg, P. C. & Coates, P. D. Nano-scale temperature dependent visco-elastic properties of polyethylene terephthalate (PET) using atomic force microscope (AFM). *Micron* **44**, 174-178, doi:http://dx.doi.org/10.1016/j.micron.2012.06.004 (2013).

20 Grant, C. A., Brockwell, D. J., Radford, S. E. & Thomson, N. H. Tuning the Elastic Modulus of Hydrated Collagen Fibrils. *Biophysical Journal* **97**, 2985-2992, doi:10.1016/j.bpj.2009.09.010.

21 Grant, C. A., Twigg, P. C., Savage, M. D., Woon, W. H. & Greig, D. Mechanical Investigations on Agar Gels Using Atomic Force Microscopy: Effect of Deuteration. *Macromolecular Materials and Engineering* **297**, 214-218, doi:10.1002/mame.201100164 (2012).

22 Grant, C. A. *et al.* Estimating the Mechanical Properties of Retinal Tissue Using Contact Angle Measurements of a Spreading Droplet. *Langmuir* **29**, 5080-5084, doi:10.1021/la400650t (2013).

23 Dobb, M. G., Robson, R. M. & Roberts, A. H. The ultraviolet sensitivity of Kevlar 149 and Technora fibres. *Journal of Materials Science* **28**, 785-788, doi:10.1007/bf01151257 (1993).

24 Carlsson, D. J., Gan, L. H. & Wiles, D. M. Photodegradation of Aramids. II. Irradiation in Air. *Journal of Polymer Science* **16**, 2365-2376 (1978).

25 Xing, Y. & Ding, X. UV Photo-stabilization of Tetrabutyl Titanate for Aramid Fibers via Sol-Gel Surface Modification. *Journal of Applied Polymer Science* **103**, 3113-3119 (2006).

Figures

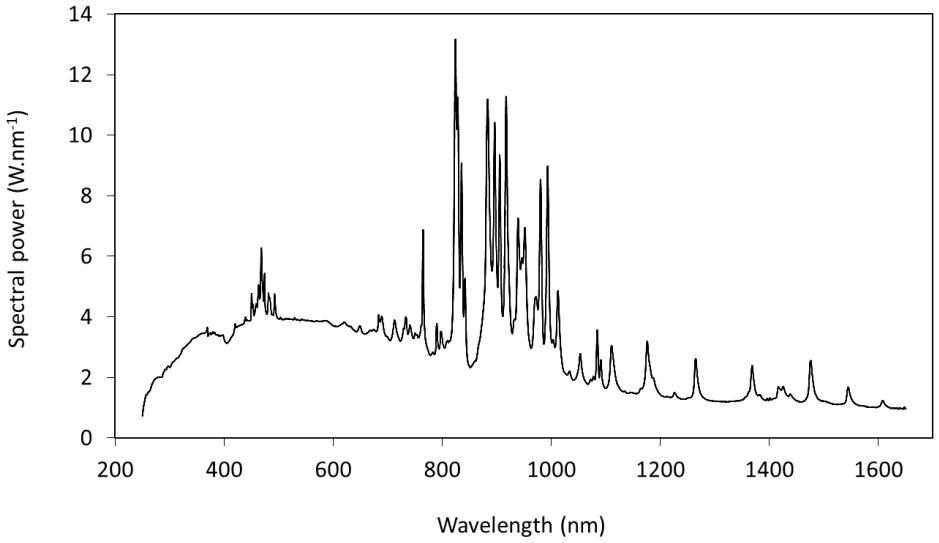

Figure 1 XBO 450 w/4 spectra (data from OSRAM Licht AG)

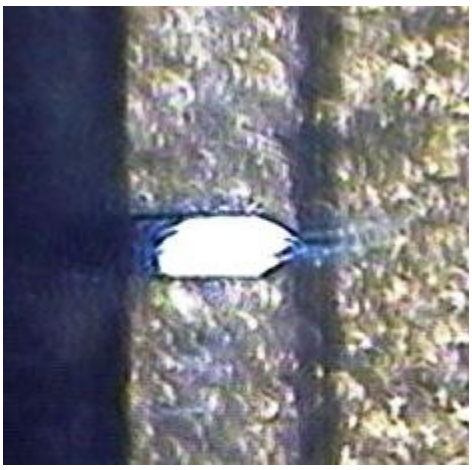

Figure 2: AFM cantilever aligned above the central aspect of a PPTA fibre

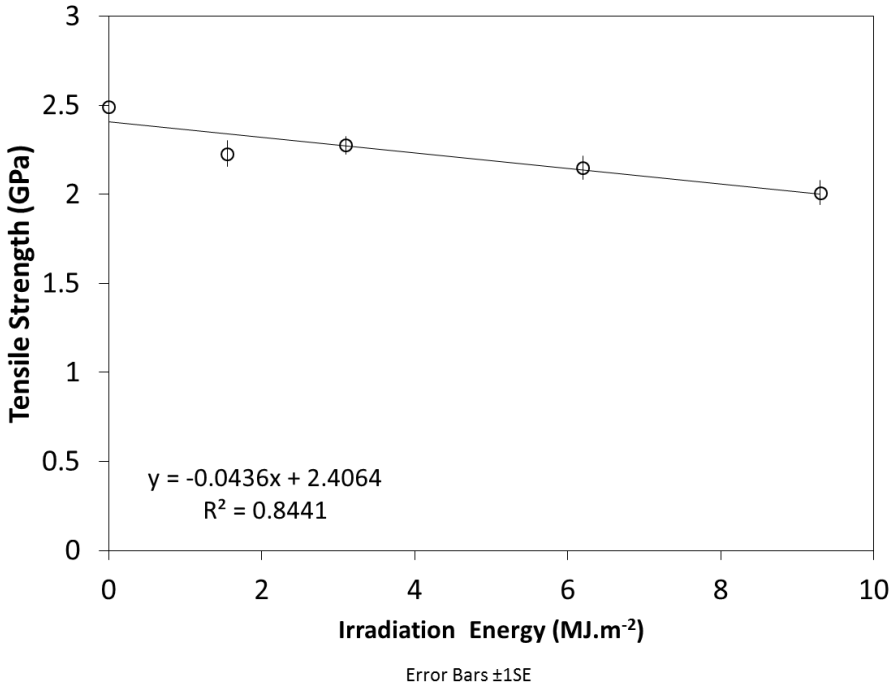

Figure 3: Effect of Irradiation Energy on Fibre Tensile Strength

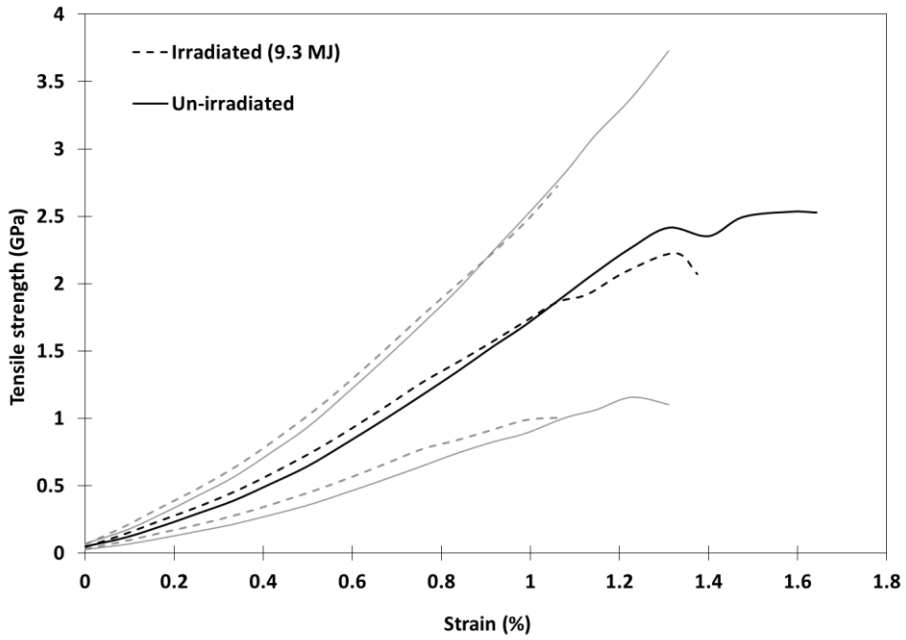

Figure 4: Average stress strain curves for non-irradiated and irradiated single PPTA fibres (upper and lower confidence limits (95%) are shown in light grey)

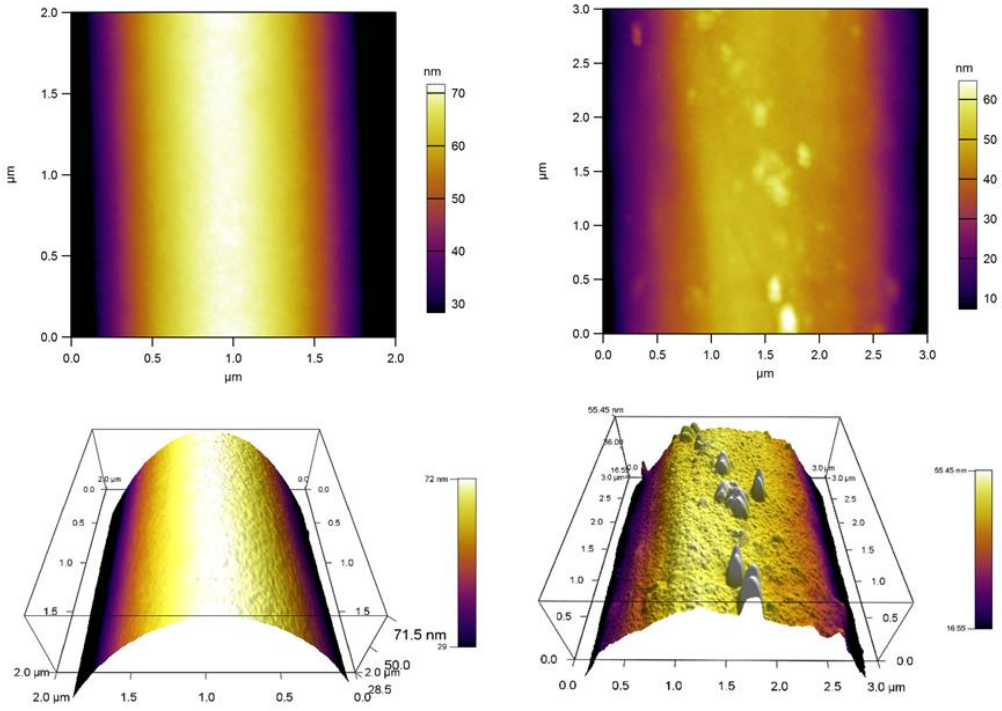

Figure 5: AFM images of non-irradiated and irradiated (76 $MJ.m^{-2}$) PPTA fibre samples with corresponding 3D representations

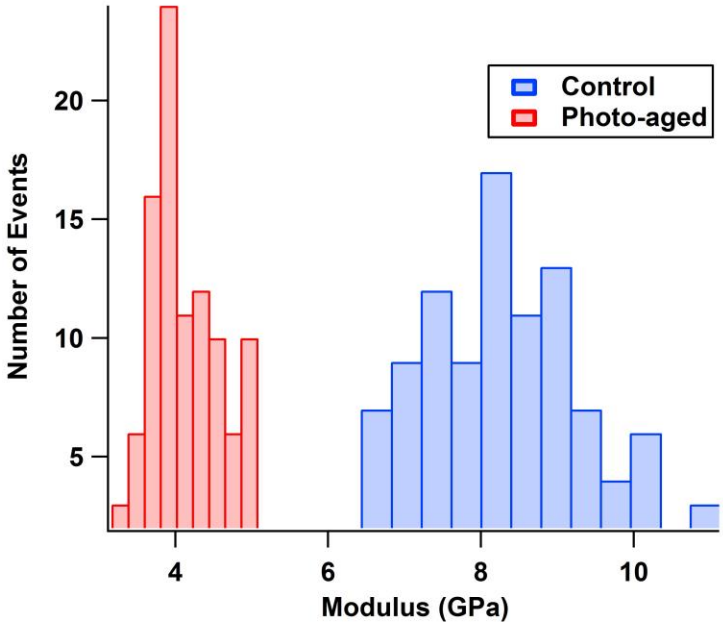

Figure 6: Distributions of nanoindentations made on the non-irradiated and irradiated PPTA fibres (76 MJ.m^{-2})

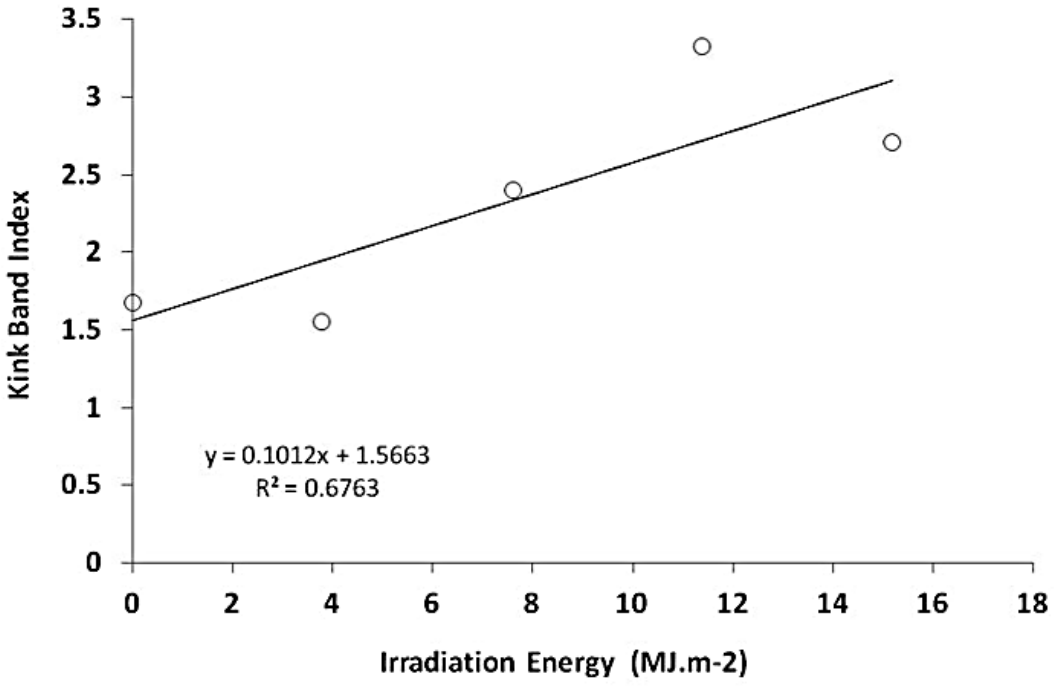

Figure 7: Kink Band Index Vs Irradiation Energy (MJ.m^{-2})

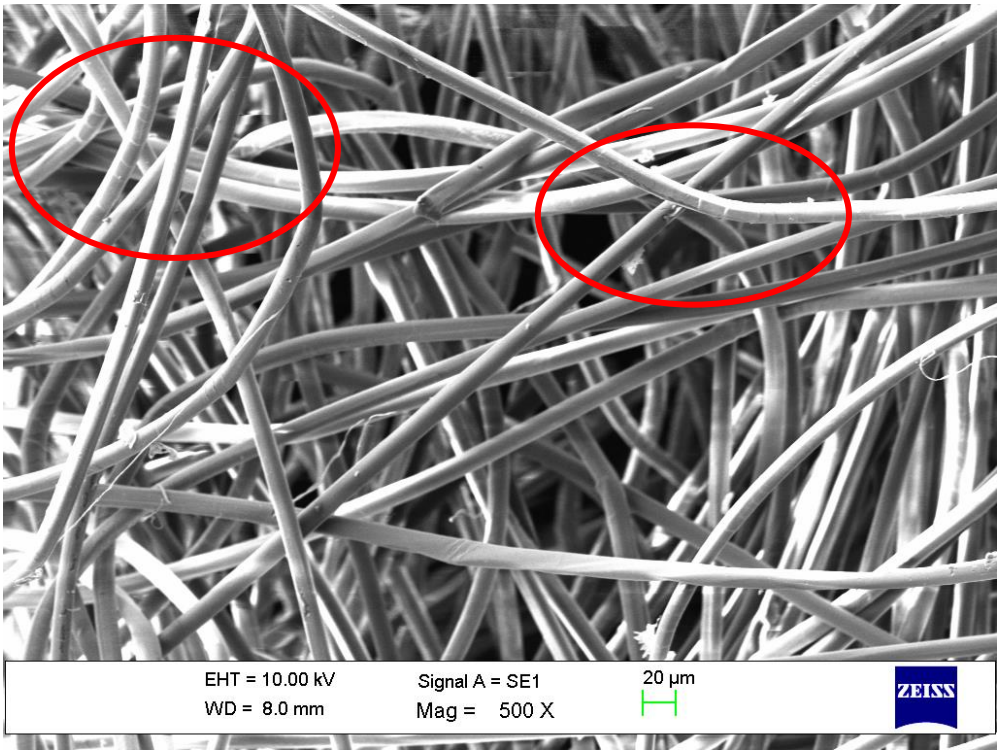

Figure 8: SEM Image of non-irradiated hydroentangled PPTA fabric sample

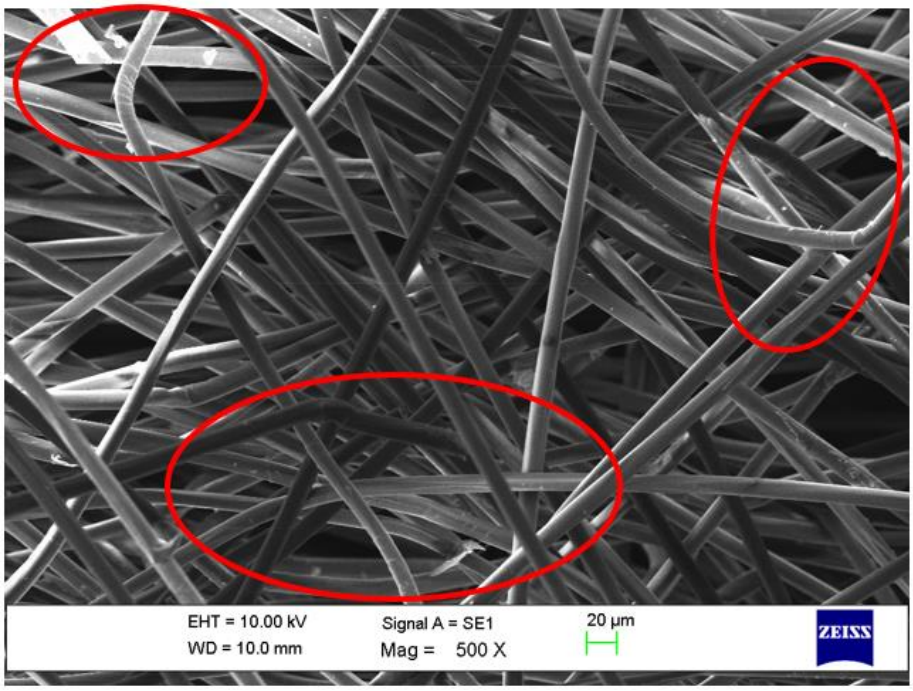

Figure 9: SEM Image of hydroetangled farbric containing irradiated PPTA (7.59 $MJ.m^{-2}$)

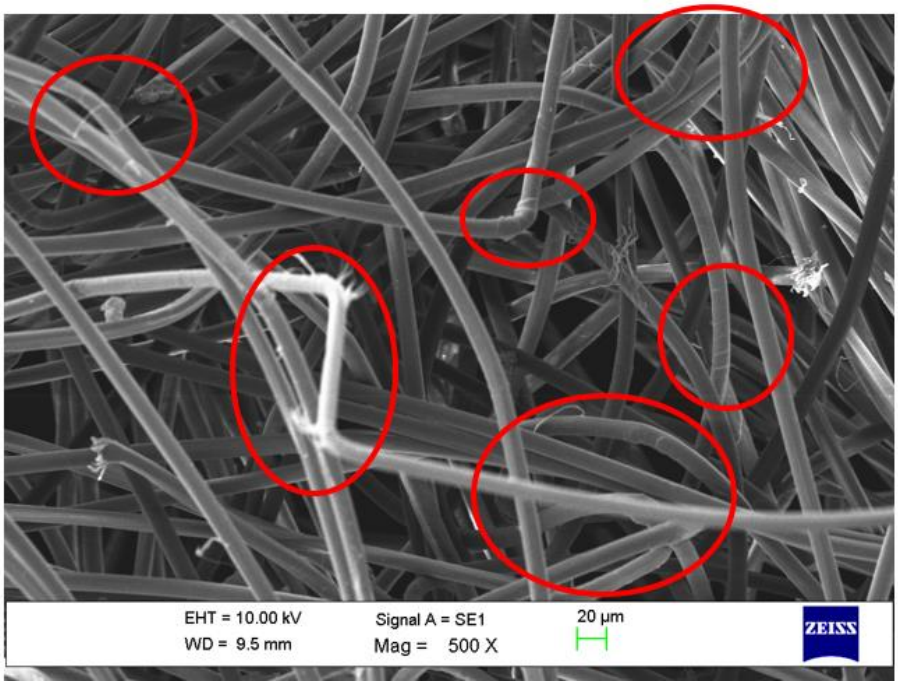

Figure 10: SEM image of hydroentangled fabric sample containing irradiated PPTA fibre (15.18 $MJ.m^{-2}$)

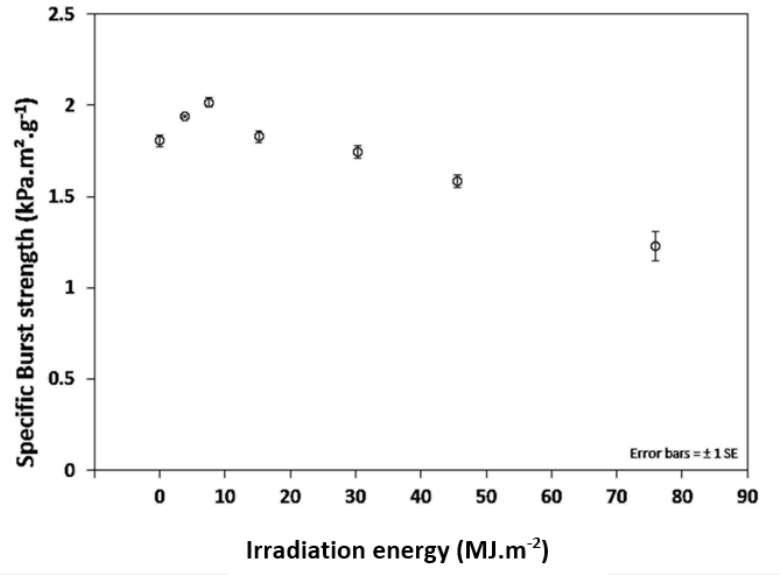

Figure 11: Specific bursting strength vs. irradiation energy (error bars ± 1 SE)

Tables

Table 1: Summary of hydroentangling process settings

Belt speed ($m.min^{-1}$)	5
Water pressure (MPa)	10
Jet orifice diameter (μm)	150
Jet orifice density (m^{-1})	1001
Jet orifice pitch (mm)	0.5

Table 2: Elastic modulus of the control (non-irradiated) and irradiated single fibres ($9.3\ MJ.m^{-2}$).

	Non-Irradiated ($0\ MJ.m^{-2}$)	Irradiated ($9.3\ MJ.m^{-2}$)
Mean elastic modulus, E (GPa)	82.5	80.9
Standard deviation	6.8	9.9